

## Article

# Fabrication of the $\text{Cu}_2\text{ZnSnS}_4$ Thin Film Solar Cell via a Photo-Sintering Technique

Vu Minh Han Cao <sup>1</sup>, Jaesung Bae <sup>1</sup> , Joongpyo Shim <sup>2</sup>, Byungyou Hong <sup>1</sup>, Hongsub Jee <sup>1,\*</sup> and Jaehyeong Lee <sup>1,\*</sup> 

<sup>1</sup> Department of Electrical and Computer Engineering, Sungkyunkwan University, Suwon 16419, Korea; cvmhan2002@gmail.com (V.M.H.C.); ba0228@skku.edu (J.B.); byhong@skku.edu (B.H.)

<sup>2</sup> Department of Nano and Chemical Engineering, Kunsan National University, Kunsan 54150, Korea; jpshim@kunsan.ac.kr

\* Correspondence: hsjee@skku.edu (H.J.); jaehyeong@skku.edu (J.L.)

**Abstract:** Alternative photo-sintering techniques for thermal annealing processes are used to improve the morphology, layer properties, and enhance solar cell performance. The fast, nontoxic, low cost, and environmentally friendly characteristics of  $\text{Cu}_2\text{ZnSnS}_4$  have led to its consideration as an alternative potential absorber layer in copper indium gallium diselenide thin film solar cells. This work investigates the photo-sintering process for the absorber layer of  $\text{Cu}_2\text{ZnSnS}_4$  solar cells. A  $\text{Cu}_2\text{ZnSnS}_4$  layer was grown by hot-injection and screen-printing techniques, and the characteristics of the photo-sintered  $\text{Cu}_2\text{ZnSnS}_4$  layer were evaluated by X-ray Diffraction, Raman spectroscopy, Energy dispersive X-ray analysis, Ultraviolet-visible spectroscopy, and field emission scanning electron microscopes. Overall, the optimal composition was Cu-poor and Zn-rich, without a secondary phase, estimated optical band-gap energy of approximately 1.6 eV, and enhanced morphology and kesterite crystallization. Using an intensity pulse light technique to the CZTS layer, fabrication of the solar cell device demonstrated successfully, and the efficiency of 1.01% was achieved at 2.96 J/cm<sup>2</sup>.

**Keywords:** CZTS solar cell; hot-injection; photo-sintering; Intense Pulse Light System



**Citation:** Cao, V.M.H.; Bae, J.; Shim, J.; Hong, B.; Jee, H.; Lee, J. Fabrication of the  $\text{Cu}_2\text{ZnSnS}_4$  Thin Film Solar Cell via a Photo-Sintering Technique. *Appl. Sci.* **2022**, *12*, 38. <https://doi.org/10.3390/app12010038>

Academic Editor: Amjad Anvari-Moghaddam

Received: 30 October 2021

Accepted: 16 December 2021

Published: 21 December 2021

**Publisher's Note:** MDPI stays neutral with regard to jurisdictional claims in published maps and institutional affiliations.



**Copyright:** © 2021 by the authors. Licensee MDPI, Basel, Switzerland. This article is an open access article distributed under the terms and conditions of the Creative Commons Attribution (CC BY) license (<https://creativecommons.org/licenses/by/4.0/>).

## 1. Introduction

Production of copper indium gallium diselenide (CIGS) solar cells is limited because indium and gallium are facing supply shortages and cost increases from competition with other manufacturing sectors, such as the display industry. In response to this, kesterite materials using  $\text{Cu}_2\text{ZnSnSe}_4$ ,  $\text{Cu}_2\text{ZnSnS}_4$  (CZTS), and  $\text{Cu}_2\text{ZnSn(S,Se)}_4$  have been evaluated as potential alternatives for chalcopyrite absorber materials, given their similar device structure to CIGS, with comparable cost reduction and increased production with the use of naturally abundantly and non-toxic materials [1]. These CZTS absorbers are semiconducting with a large optical absorption coefficient of 104 cm<sup>-1</sup> and a direct band gap of 1.13 eV for a high conversion efficiency of 12.6% [2], which allows for a layer with a thickness of a few microns. CZTS is a p-type semiconductor material comprised of abundant materials, lower toxicity, and good photovoltaic properties; as a result, kesterite crystals are potential candidates for photovoltaic devices, especially for solar cells [3,4]. Generally, greater solar cell performance requires optimal band gaps, high absorption coefficients, enhanced transport properties, long carrier lifetime, improved doping, and respective conduction band offset of the heterojunction interface [5,6].

CZTS is a p-type, I<sub>2</sub>-II-IV-VI<sub>4</sub> quaternary compound semiconductor with a crystal structure that consists of kesterite and wurtzite. Despite several advantages, the kesterite structure has lower energy and stability. The crystal structure of CZTS is similar to that of chalcopyrite CIGS, and the self-doped formation produces intrinsic defects such as vacancies, antisite defects, and interstitial defects. A p-type CZTS semiconductor commonly occurs from CuZn antisite defects caused by the Cu-poor and Zn-rich status of high-performance CZTS solar cells [7]. Additionally, specific CZTS synthesis is required

because of harmful secondary phases that are quickly formed in nonstoichiometric growth conditions, and the CZTS phase is an essential requirement for achieving high-efficiency solar cells [8]. The optical bandgap of kesterite CZTS varies with deposition method. The segregated secondary phases observed in the CZTS samples are CZTS, CTS,  $\text{Cu}_2\text{S}$ ,  $\text{CuS}$ ,  $\text{SnS}$ ,  $\text{SnS}_2$ , and  $\text{ZnS}$  [9]. The CZTS phase is very complex, with narrow phase stability that is not easy to control during synthesis [1].

Hot injection method has been used to synthesize various types of nanoparticles (NPs) with different types of metal oxides and semiconductors. Non-vacuum fabrication NPs of this method are inexpensive and easily combined with screen printing, which is a promising technique because it is simple, fast, and can be applied over a large scale for module production. This method can control the size, uniformity, composition, phase formation, and morphology of NPs. The growth mechanism is dissolution of small crystals and re-deposition of solvent on the surface of larger crystals. After introduction of a rapid injection precursor solution, the concentration of nuclei and the particles grow quickly, forming larger nuclei [10,11].

Thermal annealing is an important step during manufacturing, which significantly affects the morphology, ameliorates the interface properties of the material, and eliminates the recombination centers at the p–n junction interface [12–14], but some devices have temperature restrictions of a few hundred degrees Celsius and cannot be applied. A photo-sintering technique is an alternative thermal annealing process that is useful for temperature-sensitive materials and restrictive energy demand for a thermal process. The intense pulsed light (IPL) technique is flashlight sintering and photonic sintering that use photosensitivity to enhance crystallization, increasing the grain size of the film via small particles coalescence, and improving the junction interface state by transmission of high-energy light for rapid thermal annealing of a large area [15]. Modification of the chemical and solid states causes a sufficient heating change after a few milliseconds. The IPL technique uses instantaneous heating by fast pulses, with a usual spectrum range of 190–1100 nm created by a xenon source. The applied voltage controls the energy density of light that was transferred by electric to optical radiation of ultraviolet-visible (UV-vis) near infrared light. The energy density can be changed by parameters of the IPL system such as bank voltage, pulse number, pulse duration, pulse frequency, and number of repeats [16].

In this research, we demonstrated a photo-sintering technique as a potential candidate to replace the conventional thermal annealing process of CZTS thin film devices. This technique is adaptable for the flexible substrate and environmentally benign process, which allows usage in broad applications. Using the hot-injection, screen-printing, and IPL, CZTS NPs were applied to fabricate a photo-sintered CZTS thin film solar cell. With an energy density of  $2.96 \text{ J/cm}^2$  sintering condition, a fabricated solar cell device exhibited the 1.01% cell efficiency; this result demonstrates that light irradiation plainly sintered the CZTS film and its potential usage as a new approach for making flexible solar cell devices.

## 2. Materials and Methods

CZTS NPs were prepared by hot-injection methods from the Schlenk line. The Cu, Zn, and Sn sources were 0.133 mmol copper (II) acetylacetonate, 0.915 mmol zinc acetylacetonate, and tin (IV) bis (acetylacetonate) dichloride, respectively. The precursors were dissolved in oleylamine under purging with nitrogen gas at RT three times. The sulfur-OLA solution was heated to  $60 \text{ }^\circ\text{C}$  and injected into a flask at  $130 \text{ }^\circ\text{C}$  under nitrogen gas. This reaction was maintained for 10 min, and then the temperature was increased to  $225 \text{ }^\circ\text{C}$  for 30 min. After the finished process, the flask was cooled to RT, and NPs were washed with hexane, isopropanol, and methyl alcohol. The solution was centrifuged at 8000 rpm for 5 min to separate the CZTS NPs and remove the solvent. The powder was dried under an inflow of 4 sccm nitrogen gas.

To apply the CZTS NPs on the substrate, CZTS ink was formed by dispersion of CZTS NPs in 1-hexanethiol at 200 mg/mL. The deposited CZTS thin film was dried at  $80 \text{ }^\circ\text{C}$  for 10 min, followed by  $150 \text{ }^\circ\text{C}$  for 5 min, and then the photo-sintering process was applied.

The IPL system (PulseForge 3300, NovaCentrix; Austin, US) was used to perform the photo-sintering process, and the CZTS films were irradiated with different bank voltages while pulse duration was fixed for 1 ms. The preferential orientation and crystallinity of the films were studied by X-ray diffraction (XRD) measurements. Also, the film surface morphology was examined by an ultrahigh-resolution field emission scanning electron microscopy (FE-SEM). A Raman study was conducted using an inVia Raman microscope and a 50 mW air-cooled argon ion laser was used to excite the samples at 514 nm. The UV-vis spectrophotometry was used to measure the optical properties at wavelengths from 200 to 1000 nm.

To fabricate a solar cell device, the photo-sintered CZTS film was deposited on the Glass/Mo substrate using the CZTS ink. The film of CZTS was coated with the single-step screen printing on the substrate using a doctor-blade with the thickness of 1.5  $\mu\text{m}$ . Figure 1 illustrates the coated CZTS thin films, which were treated by the IPL for rapid thermal processing. The thin films absorbed the energy and the exposed areas resulted in a rapid rise in temperature, heated locally. This led to the metal nanoparticle films undergoing solid state and chemical modifications, becoming conductive bulk films. By controlling the energy, the CZTS films were irradiated with an energy density of 2.82, 2.96, and 3.09  $\text{J}/\text{cm}^2$ , respectively. After irradiation, a CdS buffer layer was deposited on the CZTS layer using a chemical bath deposition process. Radiofrequency (RF) magnetron sputtering formed another buffer layer of intrinsic zinc oxide (i-ZnO) (50 nm) and a high-conductivity window material of aluminum-doped zinc oxide (AZO) (500 nm). Finally, 500 nm of Al front contact was deposited by a thermal evaporator, and the area of the 0.39  $\text{cm}^2$  solar cell device was fabricated.

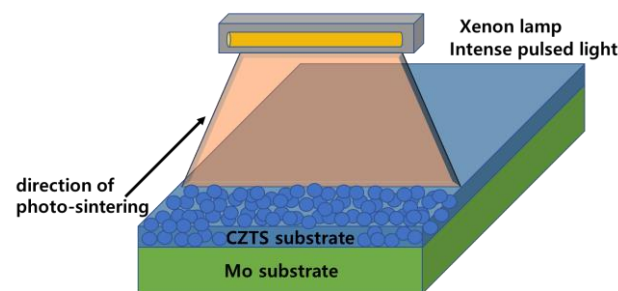


**Figure 1.** A schematic diagram of the intense pulsed light system.

### 3. Results and Discussion

The photo-sintered CZTS films have a large absorption wavelength range, as displayed in Figure 2, from 400 to 1400 nm. An optical band gap results from the extrapolated value  $h\nu$  in the x-axis at 0 of  $(\alpha h\nu)^2$ , providing the corresponding 1.6 eV that was used for the direct band gap materials. A strong absorbance was presented in the visible range, and a tail extended to longer wavelengths in the infrared region. In the visible range, CZTS has good absorption, indicating it as appropriate absorber layer of a photovoltaic device [17]. The photo-sintering process influenced the material characteristics similar to other studies [14,18,19].

Figure 3 demonstrates the surface of the as-deposited and photo-sintered CZTS films at various conditions. The as-coated CZTS film had a porous morphology with a uniform distribution of agglomerated grains and very small grains of several tens of nm. Generally, as the grain size and crystallinity improved, the CZTS surface was rougher and had island-like growth because of the increased bank voltage in the photo-sintering process. As illustrated in Figure 3, when the IPL energy increased, the particle sizes of the CZTS film also increased, which implies that crystallization occurred in the CZTS film. Increasing the energy density, duration, or repeat times causes serious destruction to the CZTS layer, as the high-energy density photo-sintered process causes peeling and cracking of the film. This damage significantly affects cell performance; so, optimization of sintering condition is necessary.

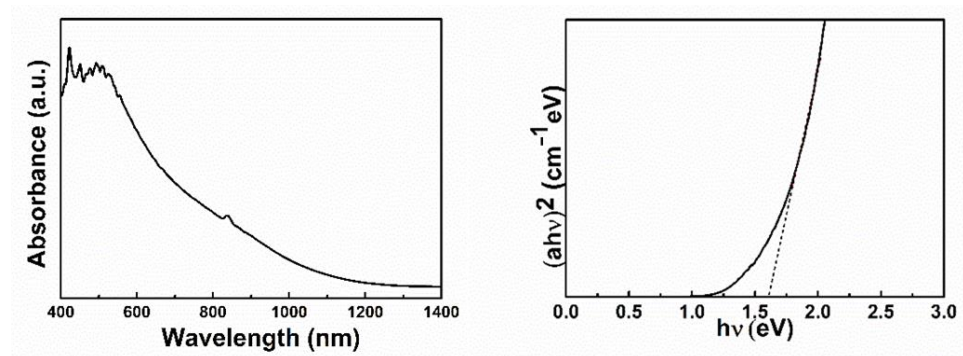


**Figure 2.** UV-vis-NIR absorption spectra of the as-coated CZTS thin film and corresponding  $(\alpha hv)^2$  vs.  $h\nu$  curve.

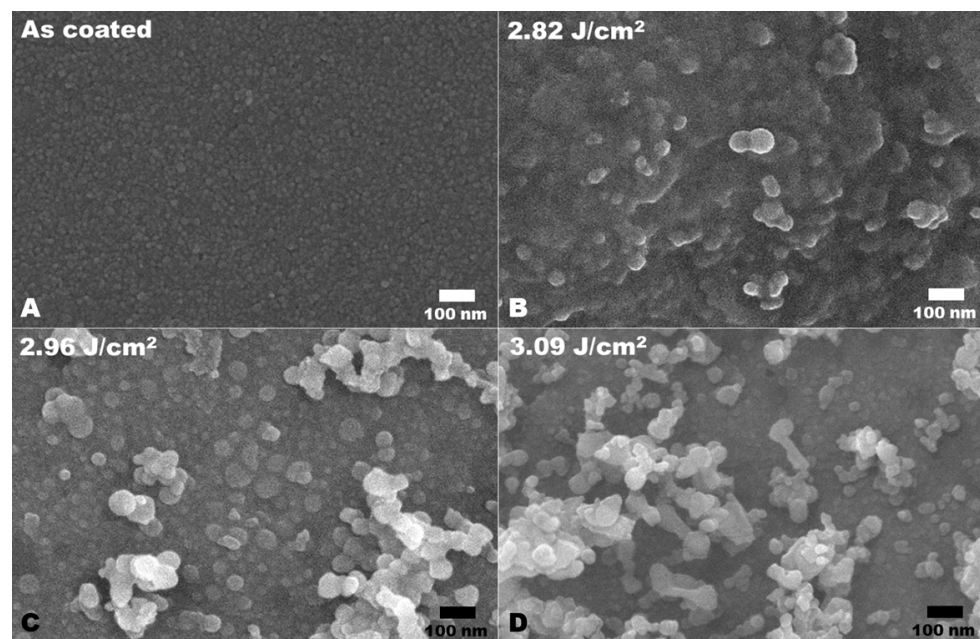


**Figure 3.** FE-SEM images of the CZTS thin film. (A) As-coated, sintered with light intensity of. (B) 2.82 J/cm<sup>2</sup>, (C) 2.96 J/cm<sup>2</sup>, (D) 3.09 J/cm<sup>2</sup>.

For the analysis of the sintering effect to the CZTS films, the XRD analysis was performed. Figure 4 displays the XRD patterns of CZTS films at various treatment conditions. As illustrated, the peaks of the (112), (200), (105), (220), and (312) planes, corresponded to the kesterite structure and verified the presence of CZTS for as-coated along with photo-sintered films [20,21]. As demonstrated in the figures, the broadening of the peaks in the XRD analysis displayed small-sized particles and the films exposed to more energy tended to have larger NPs sizes. Also, the XRD pattern broadening for the film demonstrates the surface diffusion of NPs without changing its dimension. The intensity of the diffraction peaks changes following increased energy photo-sintering application. The intensity of the peaks indicating the (112) and (220) orientations present an improvement in crystallinity of the CZTS thin films, which gradually increases at 2.82 J/cm<sup>2</sup> and decreases at higher bank voltages of 2.96 J/cm<sup>2</sup> and 3.09 J/cm<sup>2</sup>. This results in the transformation of the compound ratio and crystal structure, similar to the FE-SEM and energy dispersive X-ray analysis (EDX) results. The secondary phases consisting of ZnS, Cu<sub>2</sub>S, and Cu<sub>3</sub>SnS<sub>4</sub> are difficult to observe with XRD. As a result, Raman measurements of the CZTS thin film after treatment were performed, as illustrated in Figure 5. Raman spectroscopy provided a detailed analysis of the material compounds. The advantage of this measurement is observation of secondary phases that influence the performance of the CZTS solar cells

because of difficulty in band alignment or mismatch in structure. A 532 nm laser was used to study the CZTS thin film at a range of 200–600  $\text{cm}^{-1}$ . The formation was determined on the basis of one strong peak at 288  $\text{cm}^{-1}$  and two weak peaks at 368  $\text{cm}^{-1}$ , which closely represent the kesterite CZTS structure in other reports, and the spectra did not indicate any other characteristics peaks or secondary phases [22]. However, the main peak shifted from 329.281 to 334.345  $\text{cm}^{-1}$ , and the decrease in FWHM from 28.837 to 13.318 indicates improved crystallinity of the films with increasing energy application. The elemental compositions of these films were obtained by EDS analyses, as summarized in Tables 1 and 2. The various treatment conditions of the CZTS thin samples present a Cu-poor and Zn-rich composition with ratios of Cu/(Zn + Sn) and Zn/Sn, which are important for improving inter-diffusion in the precursor and improving the optoelectronic properties for high performance [23,24]. The dominant composition ratio occurs at 2.96  $\text{J}/\text{cm}^2$ . Increasing the bank voltage changed the composition as well as the performance of CZTS solar cells.

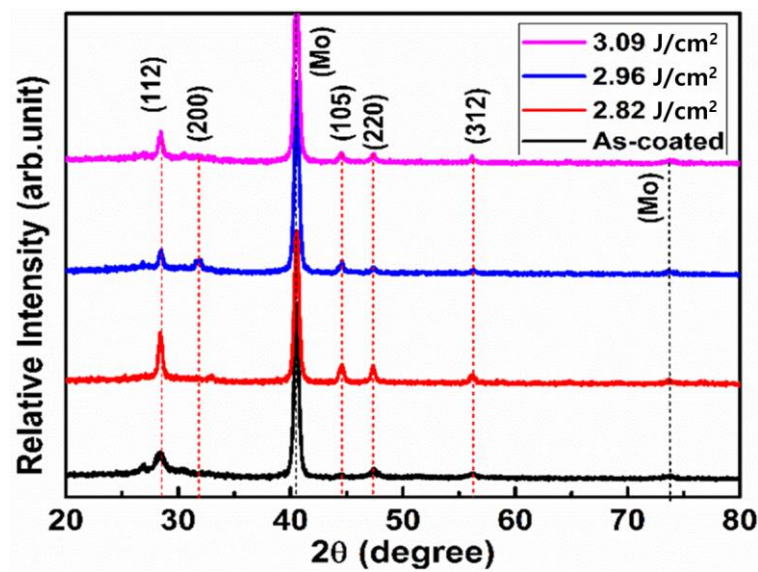


Figure 4. XRD patterns of photo-sintered CZTS thin films on molybdenum glass substrate.

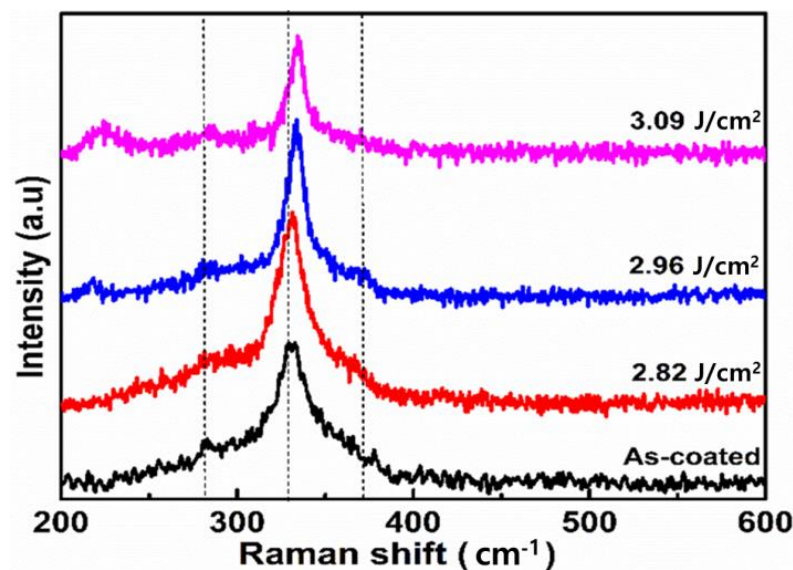


Figure 5. Raman spectrum of photo-sintered CZTS thin films on molybdenum glass substrate.

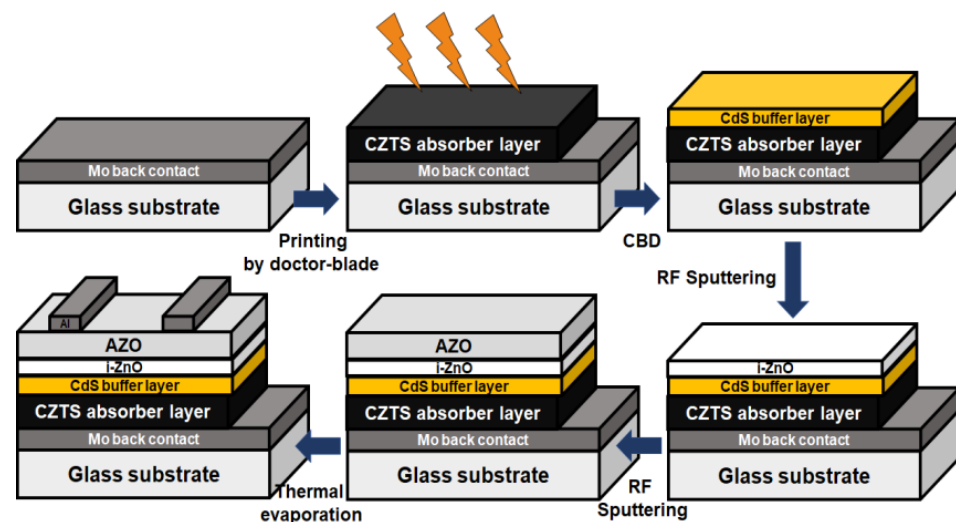
**Table 1.** Raman analysis of photo-sintered CZTS thin films at the highest peak positions.

Condition	Peak (cm <sup>-1</sup> )	FWHM
As-coated	329.281	28.837
2.82 J/cm <sup>2</sup>	331.307	22.333
2.96 J/cm <sup>2</sup>	333.838	13.642
3.09 J/cm <sup>2</sup>	334.345	13.318

**Table 2.** Chemical composition and composition ratios.

Treatment Condition	Elemental Component (at%)				Composition Ratio (at%)			
	S	Sn	Cu	Zn	Cu/(Zn + Sn)	Zn/Sn	Cu/Sn	S/Metal
As-coated	47.35	25.56	17.77	9.32	0.943	1.906	2.742	0.899
2.82 J/cm <sup>2</sup>	47.88	24.7	16.24	11.18	0.900	1.452	2.209	0.918
2.96 J/cm <sup>2</sup>	46.46	24.66	17.88	11.01	0.853	1.623	2.239	0.867
3.09 J/cm <sup>2</sup>	47.54	23.01	16.98	12.46	0.781	1.362	1.846	0.906

To analyze the performance of the applied photo-sintered film, the solar cell device was fabricated with the layer of Glass/Mo/CZTS/CdS/i-ZnO/AZO/Al. The overall fabrication process is provided in Figure 6 and the photocurrent density versus voltage (J-V) plot and performance of the photo-sintered CZTS solar cell are presented in Figure 7 and Table 3. The device with the photo-sintered CZTS film displayed a photovoltaic response, which has an energy density of 2.96 J/cm<sup>2</sup>, and exhibited the efficiency of 1.01% with an open circuit voltage (Voc) of 0.214 V, short circuit current density (Jsc) of 5.913 mA/cm<sup>2</sup>, and fill factor of 32.789%. These results clearly indicate that the light irradiation practically sintered the coated CZTS film. Using the sulfurized CZTS film, more than 10% of the efficiency were reported [25–28]; therefore, further research on applying the photo-sintering technique is required to replace the conventional thermal annealing process. Wu et al. have demonstrated that the temperature of the annealing process for CZTS film can affect the efficiency of the solar cell [29]. By controlling the light intensity and dosage, a more optimized grain size can be achieved and this may lead to high efficiency of the photo-sintered CZTS solar cell device.

**Figure 6.** Schematic of the CZTS solar cell fabrication process.

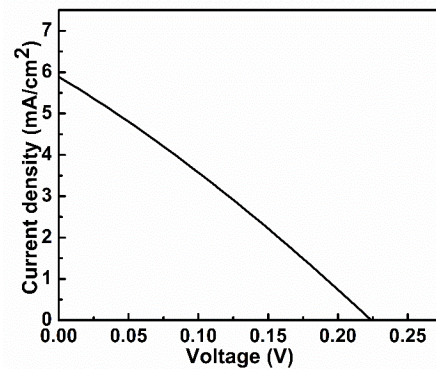


Figure 7. A J–V curve of the photo-sintered CZTS thin film solar cell.

Table 3. The measured performance of the photo-sintered CZTS thin film solar cell with CdS and ZnS buffer layers.

Condition	Voc (V)	Isc (mA/cm <sup>2</sup> )	Fill Factor (%)	Efficiency (%)	Rsh (Ω)	Rs (Ω•cm <sup>2</sup> )
2.96 J/cm <sup>2</sup>	0.224	5.913	32.789	1.01	378.713	26.417

#### 4. Conclusions

We have successfully demonstrated the photo-sintering technique for the CZTS thin film solar cell. CZTS NPs were achieved by hot injection and a screen printing method was used to apply the CZTS ink on the substrate. The photo-sintered CZTS thin film displayed a kesterite structure through XRD measurement, and a Cu-poor and Zn-rich composition for production of CZTS solar cells was also demonstrated. Raman spectrum and FE-SEM images demonstrated that the morphology and crystallization were improved after treatment. Finally, the fabricated solar cell device with photo-sintered CZTS thin films achieved 1.01% cell efficiency at an energy density of 2.96 J/cm<sup>2</sup>. The photo-sintering technique by light irradiation proves to be an important sintering tool for replacing the conventional thermal annealing process on the firm or flexible substrate with a fast and nontoxic process. Although the fabricated device displays low efficiency compared to the previous thermal sintering method, its advantages—fast processing time, low process temperature, adoptable for large areas, and suitable for flexible substrate—can open paths to various applications. The performance of the device can be enhanced by additional analysis and optimization of surface roughness, different thickness, and photo-sintering conditions of the CZTS layer. The analysis of photoluminescence spectra for reducing recombination is also necessary.

**Author Contributions:** Study design, V.M.H.C., J.B. and J.S.; experiments, J.B.; data analysis, J.S. and B.H.; writing—original draft, V.M.H.C. and H.J., writing—review and editing, H.J. and J.L.; supervision, J.L. All authors have read and agreed to the published version of the manuscript.

**Funding:** This study was supported by the Korea Electric Power Corporation (Grant number: R17XA05-1) and the National Research Foundation of Korea (NRF) grant funded by the Korea government (MSIT) (No. NRF-2019R1F1A1061615).

**Institutional Review Board Statement:** Not applicable.

**Informed Consent Statement:** Not applicable.

**Data Availability Statement:** The data that support the findings of this study are available upon reasonable request.

**Conflicts of Interest:** The authors declare no conflict of interest.

## References

1. Mukesh, K.; Ashish, D.; Nirmal, A.; Swaminathan, V.; Qiao, Q. Strategic review of secondary phases, defects and defect-complexes in kesterite CZTS–Se solar cells. *Energy Environ. Sci.* **2015**, *8*, 3134–3159.
2. Wei, W.; Mark, T.W.; Oki, G.; Tayfun, G.; Teodor, K.T.; Yu, Z.; David, B.M. Device Characteristics of CZTSSe Thin-Film Solar Cells with 12.6% Efficiency. *Adv. Energy Mater.* **2013**, *4*, 1301465.
3. Krishan, P.; Pawan, S.; Abhishikta, B.; Kenm, B.T. Current challenges and future prospects for a highly efficient (>20%) kesterite CZTS solar cell: A review. *Sol. Energy Mater. Sol. Cells.* **2019**, *196*, 138–156.
4. Swati, T.; Sadanand; Pooja, L.; Dilip, K.D. Contribution to sustainable and environmental friendly non-toxic CZTS solar cell with an innovative hybrid buffer layer. *Sol. Energy* **2020**, *204*, 748–760.
5. Liu, X.; Feng, Y.; Cui, H.; Liu, F.; Hao, X.; Conibeer, G.; Mitzi, D.B.; Green, M. The current status and future prospects of kesterite solar cells: A brief review. *Prog. Photovoltaics.* **2016**, *24*, 879–898. [[CrossRef](#)]
6. Andrew, F.; Eric, G.; Victor, I.; Xavier, F.; Fabian, A.P.; Osvaldo, V.; Alejandro, P.; Edgardo, S. Development of a Selective Chemical Etch to Improve the Conversion Efficiency of Zn-Rich  $\text{Cu}_2\text{ZnSnS}_4$  Solar Cells. *JACS* **2012**, *134*, 8018–8021.
7. Michael, P.; Leo, C.; Alain, L.; Catherine, G.; Stephane, J. Solid-State NMR and Raman Spectroscopy to Address the Local Structure of Defects and the Tricky Issue of the Cu/Zn Disorder in Cu-Poor, Zn-Rich CZTS Materials. *Inorg. Chem.* **2014**, *53*, 8646–8653.
8. Liu, W.; Chen, S.; Huang, C.; Lee, M.; Kuo, H. Investigation of Zn/Sn ratio for improving the material quality of CZTS thin films with the reduction of  $\text{Cu}_{2-x}\text{S}$  secondary phase. *J. Alloys. Compd.* **2021**, *853*, 157237. [[CrossRef](#)]
9. Lund, E.A.; Du, H.; Hlaing, W.M.; Teeter, G.; Scarpulla, M.A. Investigation of combinatorial coevaporated thin film  $\text{Cu}_2\text{ZnSnS}_4$  (II): Beneficial cation arrangement in Cu-rich growth. *J. Appl. Phys.* **2014**, *115*, 173503. [[CrossRef](#)]
10. Pratikshya, S.; Noah, H.; Peter, H.P.; Bin, L.; Viktor, C. Size-Controlled Synthesis of Iron and Iron Oxide Nanoparticles by the Rapid Inductive Heating Method. *ACS Omega* **2020**, *5*, 19853–19860.
11. Uma, G.; Mahesh, S.; Seung, W.S.; Kishor, G.; Pramod, P.; Sambhaji, P.; Chang, W.H.; Jin, H.K.; Sanjay, K. Towards environmentally benign approaches for the synthesis of CZTSSe nanocrystals by a hot injection method: A status review. *Chem. Commun.* **2014**, *50*, 11258–11273.
12. Han, J.; Fu, G.; Krishnakumar, V.; Liao, C.; Wolfram, J. CdS annealing treatments in various atmospheres and effects on performances of CdTe/CdS solar cells. *J. Mater. Sci. Mater. Electron.* **2013**, *77*, 2695–2700.
13. Hulya, M.G.; Ramazan, E. Annealing studies on CBD grown CdS thin films. *J. Cryst. Growth* **2003**, *258*, 141–148.
14. Chung, Y.; Cho, D.; Park, N.; Lee, K.; Kim, J. Effect of annealing on CdS/Cu(In,Ga)Se<sub>2</sub> thin-film solar cells. *Curr. Appl. Phys.* **2011**, *11*, S65–S67. [[CrossRef](#)]
15. Dharmadasa, R.; Lavery, B.W.; Dharmadasa, I.; Druffel, T. Processing of CdTe thin films by intense pulsed light in the presence of CdCl<sub>2</sub>. *J. Coat. Technol. Res.* **2015**, *12*, 835–842. [[CrossRef](#)]
16. Thad, D.; Ruvini, D.; Brandon, W.L.; Krishnamraju, A. Intense pulsed light processing for photovoltaic manufacturing. *Sol. Energy Mater. Sol. Cells* **2018**, *174*, 359–369.
17. Sonali, D.; Kadambinee, S.; Prakash, M.; Jagatpati, R.; Injamul, A.; Ramagouri, S.; Pitamber, M. Synthesis of quaternary chalcogenide CZTS nanoparticles by a hydrothermal route. *IOP Conf. Ser. Mater. Sci. Eng.* **2018**, *10*, 674–677.
18. Vu, M.H.C.; Soohyun, H.; Jian, L.; Jaehyeong, L. Performance of Cu(In, Ga)Se<sub>2</sub> Solar Cells on Zinc Sulfide Buffer Layers for Various Power Values of an Intense Pulsed Light System. *JNN* **2019**, *19*, 1635–1639.
19. Cao, V.M.H.; Hwang, S.; Lin, J.; Lee, S.; Kim, S.; Lee, J. Effects of Photosintering on Properties of Cadmium Sulfide Thin Films for Highly Efficient Cu(In, Ga)(Se, S)<sub>2</sub> Solar Cells. *SAM* **2018**, *10*, 1133–1139. [[CrossRef](#)]
20. Sekou, M.C.; Lingling, W.; Xintong, Z. Easy hydrothermal preparation of  $\text{Cu}_2\text{ZnSnS}_4$  (CZTS) nanoparticles for solar cell application. *Nanotech* **2013**, *24*, 495401.
21. Katy, H.; Bonna, K.N.; Jeffrey, L.J.; Hui, D.; Paulo, A.F.; Vardaan, C.; Trudy, B.; Bruce, M.C.; Antonio, F.C.; Glenn, T.; et al. Detection of ZnS phases in CZTS thin-films by EXAFS. In Proceedings of the IEEE 37th Photovoltaic Specialist Conference (PVSC), Seattle, WA, USA, 19–24 June 2011.
22. Ali, A.; Moiz, M.; Kamarulazizi, I.; Muhammad, A.F. Effect of sulfurization time on the properties of copper zinc tin sulfide thin films grown by electrochemical deposition. *Sci. Rep.* **2016**, *6*, 32431.
23. Hironori, K.; Kazuo, J.; Win, S.M.; Koichiro, O.; Makoto, Y.; Hideaki, A.; Akiko, T. Development of CZTS-based thin film solar cells. *Thin Solid Films.* **2009**, *517*, 2455–2460.
24. Jonathan, J.S.; Phillip, J.D.; Laurence, M.P. Towards sustainable materials for solar energy conversion: Preparation and photoelectrochemical characterization of  $\text{Cu}_2\text{ZnSnS}_4$ . *Electrochem. Commun.* **2008**, *10*, 639–642.
25. Caleb, K.M.; Wei-Chang, Y.; Charles, J.H.; Nathaniel, J.C.; Chinmay, S.J.; Eric, A.S.; Rakesh, A. 9.0% efficient  $\text{Cu}_2\text{ZnSn}(\text{S},\text{Se})_4$  solar cells from selenized nanoparticle inks. *Prog. Photovoltaics.* **2014**, *23*, 654–659.
26. Kim, K.; Pan, C.; Bansal, S.; Malhotra, R.; Kim, D.; Chang, C. Scalably synthesized environmentally benign, aqueous-based binary nanoparticle inks for  $\text{Cu}_2\text{ZnSn}(\text{S},\text{Se})_4$  photovoltaic cells achieving over 9% efficiency. *Sustain. Energy Fuels.* **2017**, *1*, 267–274. [[CrossRef](#)]
27. Wang, W.; Han, S.; Sung, S.; Kim, D.; Chang, C. 8.01% CuInGaSe<sub>2</sub> solar cells fabricated by air-stable low-cost inks. *Phys. Chem. Chem. Phys.* **2012**, *14*, 11154–11159. [[CrossRef](#)]

28. Liu, J.; Zhuang, D.; Luan, H.; Cao, M.; Xie, M.; Li, X. Preparation of Cu(In,Ga)Se<sub>2</sub> thin film by sputtering from Cu(In,Ga)Se<sub>2</sub> quaternary target. *Prog. Nat. Sci.* **2013**, *23*, 133–138. [[CrossRef](#)]
29. Zhang, P.; Yu, Q.; Min, X.; Guo, L.; Shi, J.; Zhao, X.; Li, D.; Luo, Y.; Wu, H.; Meng, Q.; et al. Fabrication of Cu<sub>2</sub>ZnSn(S,Se)<sub>4</sub> photovoltaic devices with 10% efficiency by optimizing the annealing temperature of precursor films. *RSC Adv.* **2018**, *8*, 4119–4124. [[CrossRef](#)]